Preparation and Characterization of Flame-Retardant Melamine Cyanurate/Polyamide 6 Nanocomposites by *In Situ* Polymerization

Zhi-Yong Wu,[1,2] Wei Xu,[1,2] Yao-Chi Liu,[1] Jin-Kui Xia,[2] Qian-Xin Wu,[2] Wei-Jian Xu[1]

[1]*Polymer Institute, College of Chemistry and Chemical Engineering, Hunan University, Changsha 410082, China*
[2]*Rubber Department of Baling Petrochemical Limited Liability Company, SINOPEC, Yueyang 414000, China*

Received 26 May 2008; accepted 8 January 2009
DOI 10.1002/app.30022
Published online 24 April 2009 in Wiley InterScience (www.interscience.wiley.com).

ABSTRACT: This article focuses on an improved method, i.e., improved *in situ* polymerization of ε-caprolactam in the presence of melamine derivatives to prepare flame-retardant melamine cyanurate/polyamide 6 (MCA/PA6) nanocomposites. The chemical structures of these synthetic flame retardant composites are characterized by Fourier-transform infrared spectroscopy and X-ray diffraction. Morphologies, mechanical properties, and thermal properties also are investigated by the use of transmission electron microscopy, mechanical testing apparatus, differential scanning calorimetry, and thermogravimetric analysis, respectively. Through transmission electron microscopy photographs, it can be found that the *in situ*-formed MCA nanoparticles with diametric size of less than 50 nm are nanoscaled, highly uniformly dispersed in the PA6 matrix. These nanocomposites, which have good mechanical properties, can reach UL-94 V-0 rating at 1.6-mm thickness even at a relatively low MCA loading level. © 2009 Wiley Periodicals, Inc. J Appl Polym Sci 113: 2109–2116, 2009

Key words: *in situ* polymerization; flame retardant; polyamide 6; nanocomposite

INTRODUCTION

Because of its chemical stability and superior mechanical and electrical properties, polyamide 6 (usually known as nylon 6, PA6) has many industrial uses, such as fibers for clothing and automobiles.[1,2] However, in some of these fields, it is desirable to provide this material with a high level of flame retardance in addition to its inherent properties. However, this thermoplastic with low limiting oxygen index can easily burn. Thus, how to impart flame retarding property to PA6 material becomes an important research topic.[3–15]

Among the several common used flame retardant additives, the *s*-triazine compounds, including melamine or its derivatives, have been widely studied during the past 20 years.[3–12] Because of its efficiency, small additive dosage, and small negative effect on the mechanical performance of the matrix resin, these class environmentally friendly flame retardants are widely used in polyamide fields. As far as we know, most of these flame-retardant composites are prepared by simple molten blending. Because melamine or its derivatives have poor solubility in PA6, it is difficult to obtain flame-retardant polyamide 6 (FRPA6) with good mechanical and flame retarding performance at a relative low flame retardant additive loading level. Kawasaki et al. said that even when MCA is pregrinded into a fine powder particles size of 2–3 μm, it can undergo secondary agglomeration and changes into large particles of several tens of micrometers in the process of molten blending with PA6 matrix.[3] Thus, the flame-retardant composites prepared by this way are usually unspinnable because of the existence of large MCA particles. Moreover, with the lapse of the time, melamine or its decomposition products could migrate from inside of the aforementioned composites to the surface, exhibiting a phenomenon called "blooming."[3]

This article relates to improved *in situ* polymerization for preparing synthetic MCA-based FRPA6. First, melamine/adipic acid salt and cyanuric acid/hexane diamine salt were prepared by the reaction of melamine with adipic acid and cyanuric acid with hexane diamine at aqueous environment, respectively. Then, these two kinds of salts were introduced into the hydrolytic polymerization system of ε-caprolactam to prepare MCA/PA6 nanocomposites. In this work, the structures and mechanical and flame retarding properties of these composites were fully characterized and investigated.

Correspondence to: W.-J. Xu (polymer_group@163.com).
Contract grant sponsors: Baling Petrochemical Limited Liability Company of SINOPEC.

TABLE I
Thermal Properties and Crystallinity of Pure PA6 and Synthetic FRPA6

Sample	$M_w \times 10^4$	$M_n \times 10^4$	T_m[a] (°C)	T_c[b] (°C)	ΔH_f[c] (J/g)	X_c[d] (%)	T_{dec}[e] (°C)	T_{10}[f] (°C)
Pure PA6	1.96	1.36	219	171	57.9	25.2	316	389
P-7.34	1.87	1.15	216	175	56.3	24.5	312	344
P-9.52	–	–	206	178	55.4	24.1	297	325

[a] Melting temperature.
[b] Temperature of crystallization peak.
[c] Heat of fusion.
[d] Percentage crystallinity calculated by DSC.
[e] Temperature at which a 5% weight loss occurred in N_2 with a heating rate of 10°C/min.
[f] Temperature at which a 10% weight loss occurred in N_2 with a heating rate of 10°C/min.

EXPERIMENTAL

Raw materials

The following materials were used as received: ε-caprolactam (chemically pure, supplied by Baling Petrochemical, Hunan Yueyang, China), melamine (chemically pure, supplied by Chengdu Kelong Chemical Plant, Chengdu, China), cyanuric acid (chemically pure, supplied by Shandong Wolan Chemical Plant, China), adipic acid and hexane diamine (Shenma Chemical Plant, China), PA6 (with relative viscosity of 3.2 in 98% H_2SO_4 as granulate product supplied by Baling Petrochemical), melamine cyanurate (MC50, purchased from Ciba Specialty Chemicals, Beijing, China).

Preparation of melamine/adipic acid salt and cyanuric acid/hexane diamine salt

Melamine/adipic acid salt was prepared by reaction of melamine with equimolecular amount of adipic acid at an aqueous environment under ambient temperature for an hour. The ratio of melamine/H_2O by mole was chosen as 1 : 4, by orthogonal experiment results. Cyanuric acid/hexane diamine salt was treated with cyanuric acid, hexane diamine and water (molar ratio 1 : 1 : 122.5), refluxing for an hour.

In situ polymerization of FRPA6

Synthetic MCA/PA6 nanocomposites were prepared in the hydrolytic polymerization system of molten ε-caprolactam. Heat supply was provided by an electric heater and controlled by a stainless rheostat. The synthetic FRPA6 prepared were summarized (Table I). For example, to synthesize P-7.34 (P signifies that it was prepared by *in situ* polymerization; 7.34 shows that it contained 7.34 g MCA per 100 g PA6) nanocomposite, 62.6 g of melamine/adipic acid salt, 56.4 g of cyanuric acid/hexane diamine salt, 24 mL of deionized water, and 800 g of ε-caprolactam were introduced into a GSH-2 2-L polymerization autoclave at room temperature. Then the autoclave was heated and kept at 275°C for 3 h. Finally, the system was cooled to 245°C, keeping vacuum-pumping for at least 30 min. The product was extracted with deionized water before measurement. Molecular weight by GPC: $M_w = 1.87 \times 10^4$, $M_n = 1.15 \times 10^4$.

P-9.52 was prepared in the same way described earlier, just changed the weight ratio of MCA with ε-caprolactam. For comparison, 58.7 g of MC50, 800 g of ε-caprolactam, and appropriate amount of water were added in the GSH-2 2-L polymerization autoclave to prepare P*-7.34.

Preparation of MCA/PA6 blend

To prepare MCA/PA6 blend of B-20.08 (weight ratio of MCA /PA6 is 20.08/100, B signifies blending), calculated amounts of MCA and dried PA6 were first mixed and dried with a high-speed mixer for 10 min (model:SHR-10A, Zhangjiagang Fangfeng Machinery, China). Then, they were melt-blended in a twin-screw extruder. (Five extruding region temperature: 160, 220, 240, 245, 250°C, $L/D = 40$, model: SHJ-20, Nanjing Sori Chemical Equipment, China.) The extrudate and synthetic MCA/PA6 nanocomposites were first cut into pellets, dried, and then injection molded into various specimens for flammability and mechanical property tests.

Characterization

Infrared (IR) spectra were performed with a WQF-410 Fourier transform infrared spectrometer (Beijing, China). Differential scanning calorimetry (DSC) and thermogravimetric analysis (TGA) were performed on a Netzsch STA 449C (Netzsch, Germany) at a heating rate of 10°C/min under nitrogen atmosphere. DSC was performed with a temperature ranging from 20 to 300°C and sample weight of ~ 10 mg under nitrogen atmosphere. Samples, encapsulated in aluminum pans, were heated to 300°C at a rate of 10°C/min and held for 5 min at this temperature to cancel their thermal history, then cooled to 20°C at a rate of 40°C/min. Finally, the sample was reheated to 300°C at a rate of 10°C/min. The recorded temperatures were calibrated by the use of indium as

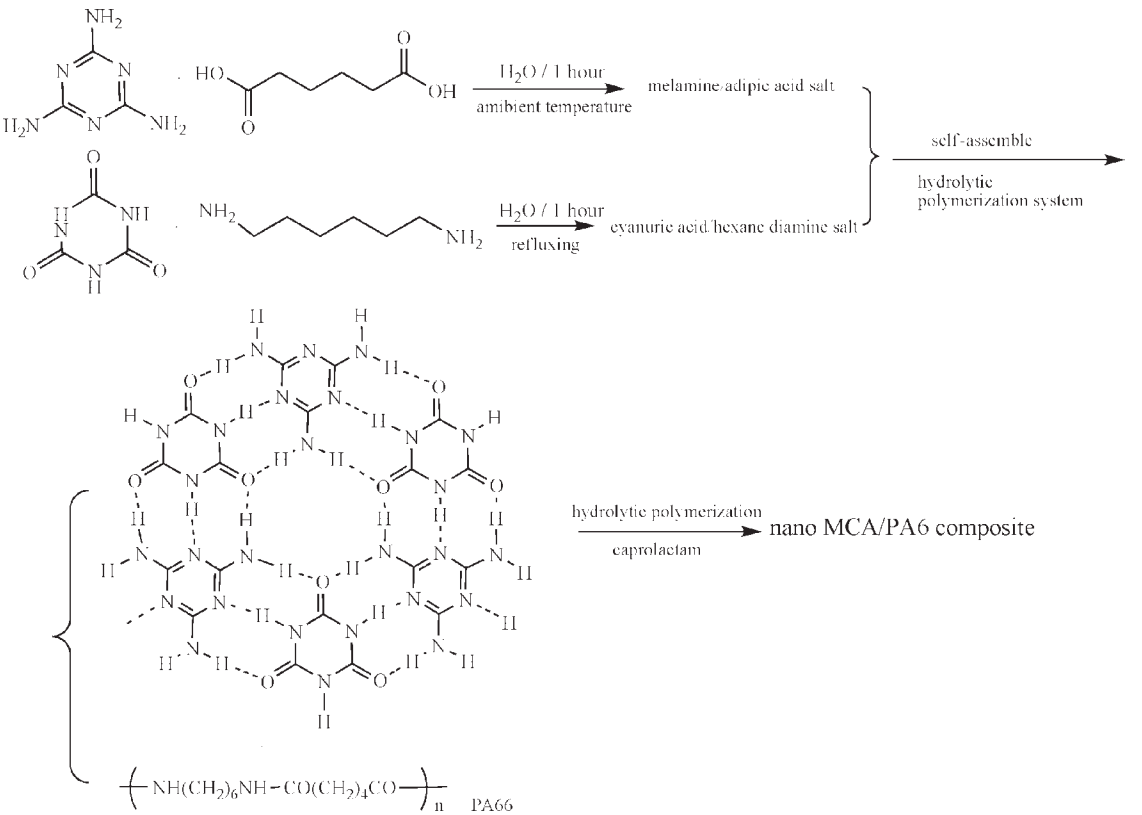

Scheme 1 Synthesis mechanisms of the MCA/PA6 nanocomposites.

standards. Crystalline melting temperature (T_m) was obtained as the maximum of the melting endotherm. Percentage crystallinity (χ_{DSC}) of products was calculated via the ratio between the measured and equilibrium heats of fusion ($\Delta H_f/\Delta H_f^0$). The equilibrium heat of fusion (ΔH_f^0) is 230 J/g for 100% crystalline PA6.[16] XRD were performed on a Rigaku D/Max2500 diffractometer (Ni-filtered, Cu/Kα radiation of wavelength 0.154 nm) in the reflection mode over the range of diffraction angles (2θ) from 5° to 45° at ambient temperature. The voltage and tube current were 40 kV and 200 mA, respectively. Gel permeation chromatography analysis was conducted on an Alltech (Altech Associate, Deerfield, IL), using polystyrene standards and *m*-cresol/chloroform mixed solvents as eluent and the flow rate was 1.0 mL/min. The morphology of the PA6 material was observed by a Hitachi Model-800 transmission electron microscope (TEM).

The vertical burning test was conducted on a CZF-3 horizontal and vertical burning tester on sheet 127 mm × 12.7 mm × 1.6 mm according to ASTM D 3801. Notched Izod impact strengths, tensile strengths, and flexural moduli were determined according to GB/T1843-1989, GB1040-1992, and GB1042-1992.

RESULTS AND DISCUSSION

Because melamine, cyanuric acid, or MCA can hardly dissolve in molten ε-caprolactam or PA6, the direct introduction of melamine and cyanuric acid into ε-caprolactam hydrolytic polymerization system can only obtain micron-grade dispersed composites,[3] whose mechanical properties are detrimentally affected. In this study, melamine/adipic acid salt and cyanuric acid/hexane diamine salt were first prepared, and their solubility in molten ε-caprolactam was much improved. Second, the two kinds of salts can self-assemble in the aqueous polymerization system to form MCA crystallites by hydrogen bonding and polycondensation reaction occurred between the left adipic acid and hexane diamine to form PA66 chains (Scheme 1).[17,18] The synthesis mechanisms of the MCA/PA6 nanocomposites are shown in Scheme 1. From the gel permeation chromatography results in Table I, it can be seen that the hydrolytic polymerization of ε-caprolactam was almost not affected by the existence of the aforementioned salts or the *in situ*-formed MCA at all. The detailed chemical structures, flame retarding performance and mechanical properties will be discussed thereinafter.

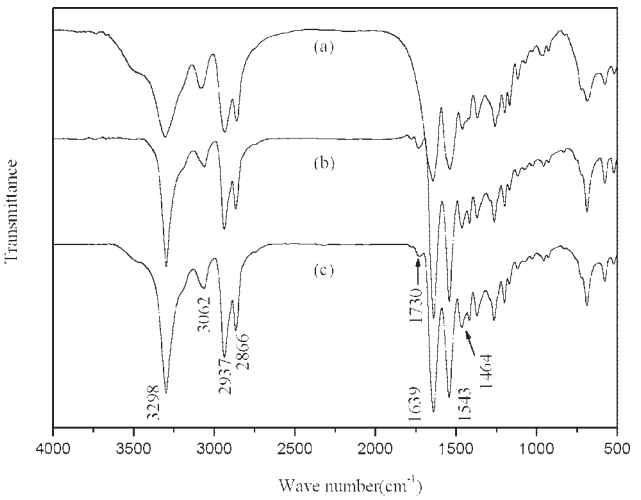

Figure 1 FTIR spectra of pure PA6 (a), MCA/PA6 nanocomposite by *in situ* polymerization (b), and MCA/PA6 composite by molten blending (c).

Structure characterization of synthesized MCA/PA6 nanocomposites

FTIR analysis

Figure 1 includes the FTIR spectra of pure PA6 [Fig. 1(a)], MCA/PA6 nanocomposite by *in situ* polymerization [Fig. 1(b), P-9.52], and FRPA6 by molten blending [Fig. 1(c), B-20.08]. It can be seen that they all display characteristic absorptions of pure PA6 at 3298 cm^{-1} (N—H stretch vibration), 1639 cm^{-1} (C=O, stretch vibration), 1543 cm^{-1} (N—H deformation). P-7.34 and B-20.08 show somewhat the same characteristic absorption bands and those characteristic absorptions of melamine and cyanuric reported (3468 cm^{-1}, 3418 cm^{-1}, stretching of —NH_2 in melamine molecule; 3027 cm^{-1}, 1467–1397 cm^{-1}, vibrations of —OH in cyanuric acid molecule, respectively.) completely disappear,[5] which indicate that the self-assembly of melamine with cyanuric is fully complete (see also in XRD patterns in Fig. 5). The band at 1464 cm^{-1} is caused by NCO and/or NCN bending coupled with ring deformation. The absorption at 1732 cm^{-1} can be attributed to the vibrations of C=O group in MCA molecule. In addition, because P-7.34 and B-20.08 own the same FTIR spectra and we can not find ester group absorption peaks, thus it can reasonably speculate the products by *in situ* polymerization are just nanoscaled MCA/PA6 composites, not star-type polymers.

DSC analysis

To compare the thermal properties of synthetic FRPA6 with pure PA6, DSC and TGA were conducted. The DSC heating curves are shown in Figure 2, where curves a, b, and c correspond to pure PA6, P-7.34, and P-9.52, respectively. For convenience, the melting and crystallizing results are presented in Table I. From Figure 2, it can be seen that all the three samples have only one endothermic peak, which corresponds to the melting of α type crystal of PA6. With the amount of MCA increases, T_m decreases from 219°C (pure PA6) to 206°C (P-9.52), but the change of percentage crystallinity is not so significant. The factors affecting the crystallization degree can be possibly attributed to the following two aspects: (1) compatibility of MCA with PA6 matrix and (2) heterogeneous nucleating effect of *in situ* formed MCA nanoparticles.[2,19] The *in situ*-formed nanoparticles in this research have strong interaction with PA6 matrix (which could be seen from TEM microscopy in Fig. 6). Therefore, with MCA content increasing, the movement of PA6 chains is restrained more greatly and the close packing of PA6 chains is interrupted, relating to more incomplete PA6 crystal. Thus, in turns of this aspect, the crystallization degree of MCA/PA6 nanocomposites should show a decreasing trend. However, at the same time, more MCA particles can enhance the heterogeneous nucleating effect, which should cause increased crystallization degree. It seems that the two aspects discussed above have contrary effects on the crystallization degree. From the experimental results, it is speculated that the first aspect plays a more important role on the little decreased trend of percentage crystallinity.

In addition, The DSC curves of pure PA6, P-7.34, and P-9.52 during cooling are presented in Figure 3 and the crystallization temperature (T_c) are listed in Table I. Compared with pure PA6, it can be seen that both samples of P-9.52 and P-7.34 have greater T_c values. It is speculated that it is caused by the heterogeneous nucleating effect of MCA

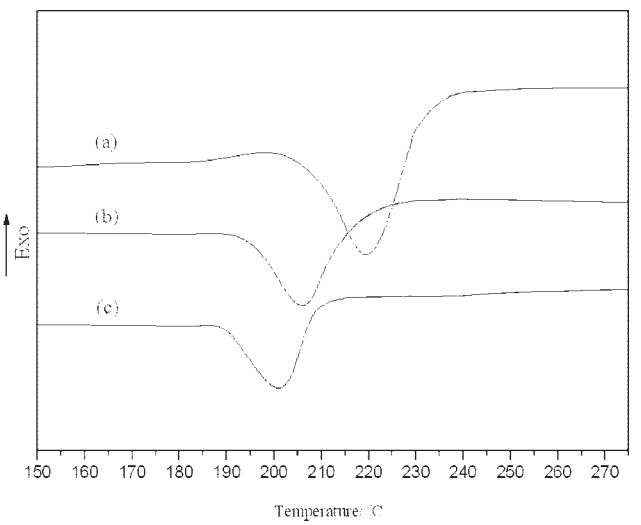

Figure 2 DSC heating curves of pure PA6 (a), flame retardant MCA/PA6 nano composites by *in situ* polymerization: P-7.34 (b), and P-9.52 (c).

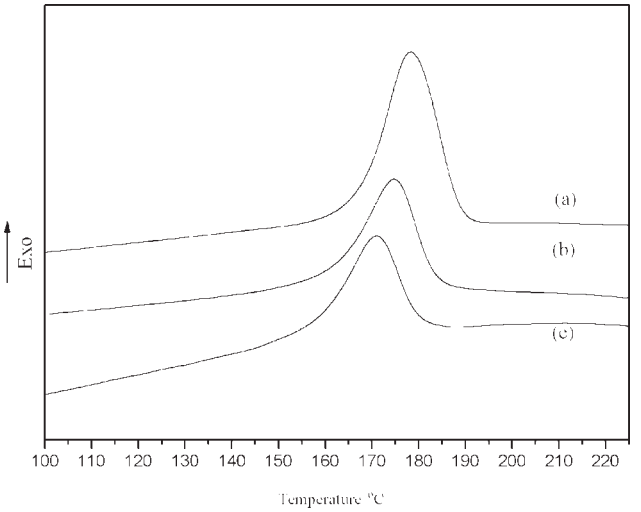

Figure 3 DSC cooling curves of flame-retardant MCA/PA6 nano composites by *in situ* polymerization: P-9.52 (a), P-7.34 (b), and pure PA6 (c).

nanoparticles in the composites. During cooling, the presence of MCA can make the molten PA6 form crystallites at a higher temperature.

TG analysis

The thermal decomposition properties of synthetic MCA/PA6 nanocomposites (P-7.34 and P-9.52) were evaluated by TGA analysis in a nitrogen atmosphere at a heating rate of 10°C/min (Fig. 4 and Table I). The decomposition temperature (T_{dec}) of P-7.34 and P-9.52 did not show significant decreasing trend, but the temperature for 10% weight loss (T_{10}), which is an important criterion for evaluating thermal stability, dramatically changed. T_{10} of P-7.34 and P-9.52 are 45°C and 64°C lower than that of pure PA6, respectively.

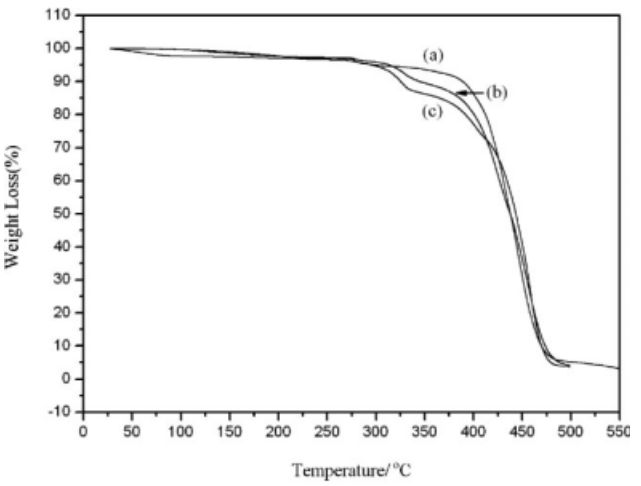

Figure 4 TG curves of pure PA6 (a) and MCA/PA6 nanocomposites: P-7.34 (b) and P-9.52 (c).

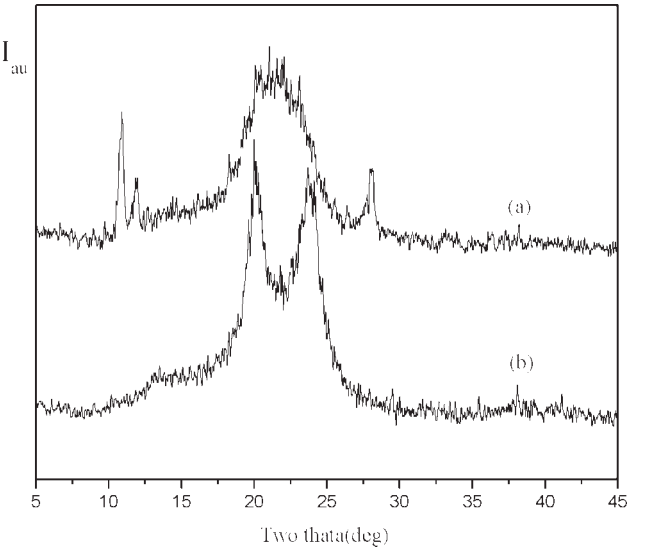

Figure 5 XRD patterns of (a) MCA/PA6 nanocomposite: P-7.34 and (b) pure PA6.

Pure PA6 weight loss takes place in a single region from 316°C to about 500°C, but the decomposition of MCA/PA6 nanocomposites involve two steps: the first one was in the range of about 300–335°C, and the second one was from 360°C to about 500°C. The first weight loss region can be reasonably attributed to the thermal dissociation of MCA to melamine and cyanuric acid, because it can be seen from Figure 4 that the curves in the first degradation region shows a weight loss proportional to MCA loading level in the composites. Also, it can be attributed to the reaction of MCA with the degradation products of PA6 because MCA can volatilize at a higher temperature when it was heated alone. The weight loss region from 360°C to about 500°C is mainly caused by the degradation of PA6 to oligomers, caprolactam, CO, etc.; the reaction of MCA (or its degradation products) with caprolactam or oligomers.

XRD analysis

Figure 5 displays the XRD patterns of P-7.34 (a) and pure PA6 (b). For curve a, characteristic MCA diffraction peaks (10.8°, 11.8°, 28.1°) appear and featured melamine and cyanuric diffraction peaks (2θ = 13.29°, 17.88°, 19.95°, 22.22°, 26.38°, 28.97°, and 29.92°) disappear,[5] indicating the self-assembly reaction becomes complete in the hydrolytic polymerization system of ε-caprolactam. For curve b, pure PA6 gives two characteristic peaks of α form at 2θ = 20.0° and 2θ = 23.8°, corresponding to the reflections of the crystalline planes (200) and (002) + (202), respectively.[20] The aforementioned analytical results are in good agreement with the FTIR results.

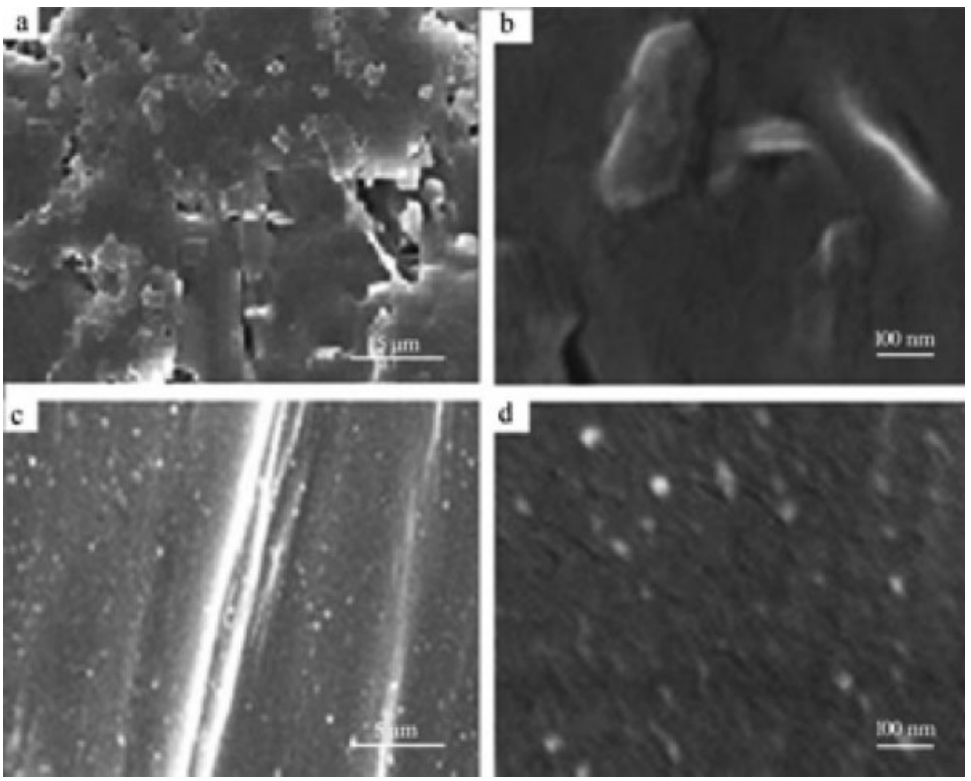

Figure 6 TEM microscopy of MCA/PA6 composite by molten blending: (a) and (b) and MCA/PA6 nanocomposite (c) and (d).

TEM analysis

TEM of FRPA6 (P-7.34) by improved *in situ* polymerization in this research is presented in Figure 6(c,d). For comparison, conventional FRPA6 by simple molten blending (B-20.08) is showed in Figure 6(a,b). From it, it is observed that the interface between conventional MCA particles and the PA6 matrix is clear. However, it becomes much more obscure for P-7.34 and the distribution is quite homogeneous. The *in situ*-formed MCA particles are nanoscaled, highly uniformly dispersed in the PA6 matrix, which can relate to much improved interfacial combination. Usually, when commercial pregrinded MCA are molten blended by an extruder or the like, fine MCA particles may undergo secondary agglomeration to form large particles, and this agglomeration can not be prevented even if a high speed extruder is used. Whereas *in situ*-formed MCA particles studied in this article are self-assembled at a relatively low rate. MCA crystallites can distribute in molten ε-caprolactam homogeneously and orientationally aligned by shear force during polymerization. Large surface area can relate to strong interface actions. So it can be predicted the synthetic FRPA6 obtained by improved *in situ* polymerization in this research should have good mechanical properties and flame retardance, which will be illuminated thereinafter.

Performance of the synthetic FRPA6

Flame retarding performance

The fire behavior has been investigated by means of the UL 94 classification (according to ASTM D3801, with dimension of 127 mm × 12.7 mm × 1.6 mm). We find that MCA/PA6 nanocomposites prepared by improved *in situ* polymerization (P-7.34, P-9.52) in this study have much better flame retarding efficiency than that of common MCA/PA6 composites by molten blending (B-20.08) or by common *in situ* polymerization (P*-7.34). P-7.34 can achieve V-0 flame retarding level at 1.6-mm thickness in the UL-94 test, and the dripping particles can not ignite the cotton fibers. Whereas in the case of MCA/PA6 blend (B-20.08), and P*-7.34, they can only achieve V-2 rating. Chen et al. have prepared MCA nanoparticle-based FRPA6 by an *in situ* extruding process.[5] In their experiments, when 7.2 and 9.0 wt % nano-MCA into PA6 matrix is incorporated, the products can not reach V-0 rating (V-2 for the former and V-0(t) for the latter). The aforementioned experiments disclose that flame retardancy is not only affected by flame retarding additive loading level, but more importantly affected by the dispersion and compatibility between the addictives and the matrix resin. In this research, the *in situ*-formed nanodispersed MCA plays a very important role in

TABLE II
Mechanical and Flame Retarding Properties of Synthetic FRPA6, Pure PA6, and PA6/MCA Blend

Sample	E_n[a] (kJ/m^2)	σ_b[b] (MPa)	E_b[c] (GPa)	σ_t[d] (MPa)	UL-94 rating
Pure PA6	13.6	91.7	2.1	66.6	V-2
P-7.34	10.4	73.1	2.2	64.1	V-0
P-9.52	8.6	62.2	2.3	60.1	V-0
P*-7.34	9.6	69.5	2.2	61.5	V-2
B-20.08	5.9	106.1	2.9	58.9	V-2

[a] Notched impact strength.
[b] Bend strength.
[c] Bend elastic modulus.
[d] Tensile strength.

improving the flame retardancy of the resulting composites. Generally, synthetic MCA/PA6 nanocomposites studied in this article have flame retarding mechanisms somewhat the same as those of common MCA/PA6 composites. During combustion, PA6 is catalyzed by MCA to degrade into low molecular weight substance, promoting the melt flow and dripping of PA6 to remove a great deal of combustion; simultaneously, the endothermic decomposition of MCA at high temperature can also decrease surface temperature and the incombustible decomposition products additionally dilute the combustible gases generated from PA6 and oxygen in the burning region, finally leading to the self-extinguishment of PA6. At last, due to the nano structure, synthetic FRPA6 in this research would display low viscosity during combustion, and crusty foam can easily form on the surface which can also insulate the remaining material from the fire and heat.

Mechanical properties

The mechanical properties of synthetic FRPA6 with different *in situ*-formed MCA loading level are listed in Table II. For comparison, the mechanical properties of pure PA6, P*-7.34, and FRPA6 by molten blending (B-20.08) are also included in it. The crystallinity and morphology of FRPA6 discussed in the previous section closely related to the mechanical properties. As can be seen, with the content of *in situ* formed MCA (from P-7.34 to P-9.52) increasing, the notched impact strength, the bend strength and the tensile strength decrease from 10.4 kJ/m^2, 73.1 MPa, and 64.1 MPa to 8.6 kJ/m^2, 62.2 MPa, and 60.1 MPa, respectively, but the bend elastic modulus increases a little. Due to the nano-scaled structure, P-7.34 owns better mechanical properties than P*-7.34. Compared with pure PA6, the incorporation of MCA can deteriorate most of the mechanical properties for both of the FRPA6 by *in situ* polymerization and by molten blending, and this deteriorating effect is less significant for the former. This can probably attribute to the much improved interfacial combination (also discussed in the TEM section). So, from the mechanical property results, it seems that the increase in MCA content may improve the flame retardancy, but is at the expense of sacrificing mechanical properties.

CONCLUSIONS

In this research, by improved *in situ* polymerization, synthetic environmentally friendly MCA/PA6 nanocomposites were prepared successfully. On the basis of the aforementioned results, the following conclusions can be drawn: the MCA crystallites, which were self-assembled in the aqueous molten ε-caprolactam, with diametric size of less than 50 nm, are highly uniformly dispersed in the PA6 matrix. From the FTIR and XRD results, it can be seen that the self-assembly reaction is complete. With the *in situ*-formed MCA nanoparticles increasing, the thermal stability shows a decreasing trend. More specifically, T_{10} of P-7.34 and P-9.52 are 45°C and 64°C lower than that of pure PA6, respectively. With the amount of MCA increasing, T_m decreases from 219°C (pure PA6) to 206°C (P-9.52), but the change of percentage crystallinity is not so significant. Because of the nanostructure, these composites can show good mechanical and flame retarding properties at relative low MCA loading level. In this research, increasing MCA content may relates to better flame retarding ability, but it would destroy the thermal stability and mechanical properties. In a word, this novel nanomaterial may provide interesting practical application in industrial fields.

The authors thank the State Key Laboratory of Chemo/Biosensing and Chemometrics, Hunan University, People's Republic of China, for their kind support for analysis.

References

1. Budin, J.; Brozek, J.; Roda, J. Polymer 2006, 47, 140.
2. Liu, Y.-C.; Xu, W.; Xiong, Y.-Q.; Zhang, F.; Xu, W.-J. Mater Lett 2008, 62, 1849.
3. Kawasaki, H.; Yoshida, K.; Itoh, T. U.S. Pat. 4,317,766, (1982).
4. Liu, Y.; Wang, Q. Polym Degrad Stab 2006, 91, 3103.
5. Chen, Y. H.; Wang, Q.; Yan, W.; Tang, H. M. Polym Degrad Stab 2006, 91, 2632.
6. Casu, A.; Camino, G.; Giorgi, M. D.; Flath, D.; Morone, V.; Zenoni, R. Polym Degrad Stab 1997, 58, 297.
7. Gijsman, P.; Steenbakkers, R.; Fűrst, C.; Kersjes, J. Polym Degrad Stab 2002, 78, 219.
8. Chen, Y. H.; Wang, Q. Polym Degrad Stab 2006, 91, 2003.
9. Galli, D.; Comense, M.; Speroni, F.; Laghetto, C. U.S. Pat. 6,608,123 (2003).
10. Chen, Y. H.; Liu, Y.; Wang, Q.; Yin, H.; Aelmans, N.; Kierkels, R. Polym Degrad Stab 2003, 81, 215.
11. Aldemaro, C.; Alberto, C. U.S. Pat. 4,321,188 (1982).
12. Moore, W. P.; Hopewell, V. U.S. Pat. 5,756,571, (1998).
13. Schartel, B.; Potschke, P.; Knoll, U.; Abdel-Goad, M. Eur Polym J 2005, 41, 1061.
14. Mehdipour-Ataei, S.; Babanzadeh, S. React Funct Polym 2007, 67, 883.
15. Liang, Y.; Xia, X. H.; Luo, Y. H.; Jia, Z. J. Mater Lett 2007, 61, 3269.
16. Crespy, D.; Landfester, K. Macromolecules 2005, 38, 6882.
17. Staniec, P. A.; Perdigao, M. A.; Rogers, B. L.; Champness, N. R.; Beton, P. H. J Phys Chem C 2007, 111, 886.
18. Bielejewska, A. G.; Marjo, C. E.; Prins, L. J.; Timmerman, P.; Jong, F. D.; Reinhoudt, D. N. J Am Chem Soc 2001, 123, 7518.
19. Hou, L. L.; Yang, G. S. Polym Bull 2006, 57, 553.
20. Ricco, L.; Russo, S.; Orefice, G.; Riva, F. Macromolecules 1999, 32, 7726.